Spin current in chemical reactions

Kota Hanasaki[1,1], Kazuo Takatsuka[1,*]

Fukui Institute for Fundamental Chemistry, Kyoto University, Takano-Nishibiraki-cho 34-4, Sakyou-ku, Kyoto, 606-8103, Kyoto,Japan

Abstract

Development in attosecond technologies has been realizing real-time control of electronic dynamics. As a useful means for real-time monitoring of radical bond-rearrangement reactions, we introduce spin flux to track the dynamics of spin density in them. As an illustrative example, we show the spin flux in the course of the basic radical reaction H· + H_2 molecule. It is demonstrated that spin flux induces spin-polarization in the molecular target (H_2) to weaken the covalent bond, thus leading to possible bond cleavage. The mechanism shown here is in harmony with the three-stage mechanism in radical reactions by Nagase et al.

Keywords: non-adiabatic dynamics, electronic current, radical reactions

1. Introduction

Spin current is among the hottest topics in material sciences. In solid-state physics, magnetic fields applied externally and/or spontaneously generated in bulk or surface of solid state materials give births to characteristic effects like the spin Hall effect that modulate the paths and amounts of current of spin, thereby the control of them sets an intense aim in spintronics [1], topological materials [2] an so on. In chemical reaction dynamics, on the other hand, studies on dynamical flows of spin density seem by far rare to the best of our knowledge. However the dynamical change of spin distribution in molecular systems, such as ultrafast electronic spin-state rearrangement in relaxation and open-shell reactions like radical chemical reactions [3, 4], electronic-state relaxation, and so on, must be of critical importance in the present and future stage of physics chemistry, in which ultrafast dynamics of spin densities is to be tracked and monitored in real time.

Spin current in a molecule is quantified in terms of the spin flux, which is the quantum-mechanical flux [5] associated with the spin density. Spin flux vanishes in even electron systems with a certain spin symmetry. For example, analogous to the parity-selection rule for the dipole operator, the spin flux vanishes between states that transform to themselves with the same sign under time-reversal symmetry [6]. Despite such restriction and others, spin flux has an important role in monitoring spin polarization [7], which can cleave the singlet pairing in chemical bonds associated with bond-rearrangement in radical reactions.

There are larger number of studies on the electronic flux in the sense of charge flux, which is now regarded as among the critical quantities that characterize the dynamics of molecular electrons [8–22]. Flux analysis has now become a standard tool for the analysis of excited state. Those studies on the dynamics of electrons within and in between molecules attain more and more importance beyond the Born-Oppenheimer paradigm. This progress has been greatly enhanced by the progress in experimental techniques such as ultrafast laser [23], which realizes real-time observation of electronic dynamics [24] and its control [25]. It is therefore of importance to re-realize that chemical changes like reactions are primarily dominated by the time propagation of electronic states. In particular, nonadiabatic electron dynamics

*Corresponding author

Email addresses: kotah@ucr.edu (Kota Hanasaki), kaztak@fukui.kyoto-u.ac.jp (Kazuo Takatsuka)

[1]Current address: Department of Chemical and Environmental Engineering, University of California, Riverside, California 92521, USA.

induces many phenomena one needs to explore including the finding of a quantum mechanical origin to break molecular optical symmetry in the Schrödinger dynamics [26], real-time dynamics of charge separation in photo-excited states in many substances and in the ground state of Mn_4CaO_5 in Photo System II [27], dynamics in highly quasi-degenerate electronic-state manifolds leading to novel chemical reactions, which is referred to as chemistry without notion of the potential energy surface [28], theory of relativity for electronic states in the space-time domain of nonadiabatic electron dynamics [29, 30], and many more as partly cited in recent review articles [31, 32]. In addition, we here are penetrating deep in electron dynamics of open-shell systems such as radical reactions.

In this paper we investigate electron spin dynamics associated with a bond-rearrangement by the means of spin flux. As an illustrative study, we work on a very basic radical reactions, H· + H_2 → H_2 + H·. Despite its seeming simplicity, the present study of the spin flux illustrates dynamical flow of spin associated with the bond rearrangement or breakage of a spin-singlet pair.

2. Theory of spin flux

The spin flux is among generalized fluxes [12] that conserve under non-relativistic Hamiltonian. It makes a contrast with many of preceding works in fluxes [8–21] which are primarily interested in the dynamics of charge degrees of freedom and/or nuclear wavefunctions. Our study also contrasts against many of existing studies on spin currents such as Refs. [22, 33] in that we are primarily interested in microscopic or atomic-scale spin fluxes induced by nuclear dynamics.

2.1. Spin flux to quantify microscopic spin current

We first introduce the notion of generalized densities and fluxes (see Ref. 12 for more general discussions) and define a generalized density operator by

$$\hat{\rho}^{\eta}(\mathbf{r}) \equiv \hat{\psi}_{\sigma}(\mathbf{r})\mathcal{M}^{\eta}_{\sigma\tau}\hat{\psi}_{\tau}(\mathbf{r}), \tag{1}$$

and its associated flux operator by

$$\begin{aligned}\hat{\mathbf{j}}^{\eta} = \sum_{\sigma\sigma'}\mathcal{M}^{\eta}_{\sigma\sigma'}\frac{\hbar}{2m_e}(\hat{\psi}^{\dagger}_{\sigma}(\mathbf{r})\left[\frac{\hbar}{i}\nabla - \frac{q_e}{c}\mathbf{A}\right]\hat{\psi}_{\sigma'}(\mathbf{r}) \\ - \left(\left[\frac{\hbar}{i}\nabla + \frac{q_e}{c}\mathbf{A}\right]\hat{\psi}^{\dagger}_{\sigma}(\mathbf{r})\right)\hat{\psi}_{\sigma'}(\mathbf{r})),\end{aligned} \tag{2}$$

where $\mathbf{A}$ indicates the electromagnetic vector potential and η labels the type of density/flux; $\eta = c$, $\eta = m$, $\eta = \alpha$ and $\eta = \beta$ represent charge, spin, α electron and β electron fluxes, respectively. The associated constant matrix $\mathcal{M}^{\eta}$ are defined as $\mathcal{M}^{c}_{\sigma\tau} = \delta_{\sigma\tau}$, $\mathcal{M}^{m}_{\sigma\tau} = \sigma\delta_{\sigma\tau}/2$, $\mathcal{M}^{\alpha}_{\sigma\tau} = \delta_{\sigma,1}\delta_{\sigma\tau}$ and $\mathcal{M}^{\beta}_{\sigma\tau} = \delta_{\sigma,-1}\delta_{\sigma\tau}$. Each pair of density and flux formally conserves in a time evolution under a general non-relativistic Hamiltonian without spin-orbit coupling H^{el} (in the Heisenberg representation) in the sense

$$\frac{d}{dt}\hat{\rho}^{\eta}(\mathbf{r}) = \frac{1}{i\hbar}\left[\hat{\rho}^{\eta}(\mathbf{r}), \hat{H}^{\mathrm{el}}\right] = -\nabla\cdot\mathbf{j}^{\eta} \tag{3}$$

Hereafter in this paper, we work on field-free dynamics in which $\mathbf{A} = \mathbf{0}$.

2.2. A three-electron doublet model

As an illustrative case study, we observe spin flux in a model radical exchange reaction H· + H_2 → H_2 + H·. As for a basic electronic-state (static) theory about ground-state radical reactions, Nagase et al. [34] proposed the three-stage mechanism in their unrestricted Hartree-Fock (UHF) study of dominant electronic state configurations in radical reactions. The first two steps are essentially the requirement in the frontier orbital theory [35], that is, (i) charge transfer from a closed shell molecule (H_2 in our case) to the singly occupied orbital (SOMO) on a radical species (here H·), which requires favorable phase-matching in the HOMO-SOMO interaction, (ii) the back charge transfer from H· to the antibonding orbital of H_2 (here $1\sigma_u$ orbital), which demands favorable SOMO-LUMO interaction. And, beyond the frontier orbital theory, it finds that (iii) triplet excitation within H_2 molecule is crucial for decoupling

of the α and β pairing spins, which used to form the tight covalent bond. This decoupling is of course necessary for the bond cleavage and for such decoupled β spin electron to begin to form a new coupling with the incoming α spin electron. In the original work of Nagase, however, the UHF were used to trace the static reaction course along with the pertubation-theoretic analysis based on the initial (before reaction) RHF orbitals. Note that the time-ordering of the above three steps (i)–(iii) should depend on a system under study. No dynamical study has been performed before the present work and we here carry out nonadiabatic electron wavepacket dynamics and extract both the electron and spin fluxes as conserving quantities with which to track the reaction throughout.

We here make a similar analysis to Nagase's [34] in order to clarify the origin of non-vanishing spin flux in radical bond-rearrangement reactions. In doing so, we first suppose a general three-electron doublet model. Let us consider general three mutually orthogonal molecular orbitals (MOs) $a, b, c, \overline{a}, \overline{b}, \overline{c}, \cdots$ where the alphabetical symbols with and without overlines $a, b, c, \overline{a}, \overline{b}, \overline{c}, \cdots$ show spin-orbitals of up and down spin. We assume that, in the initial state, A and B are bound, whereas a radical C is approaching them. Denoting the *bonding and antibonding* orbitals of A-B compound by a and b, and the singly occupied orbital of C by c, an approximate wavefunction of the system can be expanded as

$$
\begin{aligned}
|\Psi\rangle = f_1 \, |a\overline{a}c \, \mathcal{C}\rangle + f_2 \left| \frac{1}{\sqrt{2}} \left(a\overline{b} + b\overline{a}\right) c \, \mathcal{C} \right\rangle \\
+ g_1 \left| \left(\frac{1}{\sqrt{6}} \left(a\overline{b} - b\overline{a}\right) c - \sqrt{\frac{2}{3}} ab\overline{c} \right) \mathcal{C} \right\rangle + \cdots
\end{aligned}
\tag{4}
$$

where the symbol $\mathcal{C}$ represents a closed shells space of doubly occupied orbitals other than a, b and c. Ket vectors in Eq. (4) represent configuration state functions (CSFs). Coefficients on CSFs, f_1, f_2, g_1, and so on in Eq. (4), take complex values; and, unless specified otherwise, single-electron orbitals are real-valued. We now see that, in Eq. (4), the CSF $|a\overline{a}c \, \mathcal{C}\rangle$ is the SCF ground state of the initial configuration. The CSF $|\frac{a\overline{b}+b\overline{a}}{\sqrt{2}} c \, \mathcal{C}\rangle$ [$|\left(\frac{a\overline{b}-b\overline{a}}{\sqrt{6}} c - \sqrt{\frac{2}{3}} ab\overline{c} \right) \mathcal{C}\rangle$] includes a pair of α and β spin excitations with the same [opposite] sign, which we hereafter refer to as a local singlet [triplet] excitation described as below. All the CSFs are subject to the total spin $S = \frac{1}{2}$.

A CSF $|\Phi_1\rangle$ is termed as a local triplet excitation of the SCF ground state $|\Phi_0\rangle$, if there is a such pair of MOs ℓ and m that satisfy $\langle\Phi_1|\hat{a}^\dagger_{\ell\uparrow}\hat{a}_{m\uparrow}|\Phi_0\rangle = -\langle\Phi_1|\hat{a}^\dagger_{\ell\downarrow}\hat{a}_{m\downarrow}|\Phi_0\rangle$. A local singlet excitation is defined in a similar way. The notion of "local triplet excitation" is not conceptually different from the "spin-asymmetric excitation" in Ref. 34 or state ${}^2\psi_2$ in Ref. 36. The only differences are that we expand the wavefunction in spin-independent orthogonal MOs, whereas Ref. 34 uses UHF analysis and Ref. 36 uses valence-bond type nonorthogonal orbitals.

We next evaluate the expectation value of a given single-electron operator $\hat{\mathcal{O}}$ by $\langle\hat{\mathcal{O}}\rangle = \langle\Psi|\hat{\mathcal{O}}|\Psi\rangle$, the flux operator being an example, which is expanded as

$$
\begin{aligned}
\langle\hat{\mathcal{O}}\rangle &= |f_1|^2 \left(O_{aa} + O_{\overline{a}\overline{a}} + O_{cc}\right) \\
&+ |f_2|^2 \left(\frac{1}{2} \left(O_{aa} + O_{\overline{a}\overline{a}} + O_{bb} + O_{\overline{b}\overline{b}}\right) + O_{cc} \right) \\
&+ |g_1|^2 \left(\frac{1}{6} \left(5O_{aa} + O_{\overline{a}\overline{a}} + 5O_{bb} + O_{\overline{b}\overline{b}}\right) + \frac{1}{3} \left(O_{cc} + 2O_{\overline{c}\overline{c}}\right) \right) \\
&+ \frac{1}{\sqrt{2}} f_1^* f_2 \left(O_{\overline{a}\overline{b}} + O_{ab}\right) + \frac{1}{\sqrt{2}} f_2^* f_1 \left(O_{\overline{b}\overline{a}} + O_{ba}\right) \\
&+ \frac{1}{\sqrt{6}} f_1^* g_1 \left(O_{\overline{a}\overline{b}} - O_{ab}\right) + \frac{1}{\sqrt{6}} g_1^* f_1 \left(O_{\overline{b}\overline{a}} - O_{ba}\right) \\
&+ \frac{1}{2\sqrt{3}} \left(f_2^* g_1 + g_1^* f_2\right) \left(O_{aa} - O_{\overline{a}\overline{a}} - O_{bb} + O_{\overline{b}\overline{b}}\right),
\end{aligned}
\tag{5}
$$

where $O_{\xi\zeta}$, labeled with spin-orbit indices ξ, ζ, is defined by $O_{\xi\zeta} \equiv \sum_{\sigma'} \int d^3\mathbf{r}' \boldsymbol{\varphi}^*_\xi(\mathbf{r}', \sigma') \hat{\mathcal{O}} \boldsymbol{\varphi}_\zeta(\mathbf{r}', \sigma')$. The latter three terms in Eq. (5), with coefficients including both f_i and g_1, represent contributions of the cross terms of the local-triplet excitation and the SCF ground state or its local-singlet excitation. We find that those terms vanish if $\hat{\mathcal{O}}$ is a spin-independent observable or a nonlocal operator such as the

total spin population with $O_{aa} - O_{bb} = 0$, whereas they take nonvanishing value in general if $\hat{\mathcal{O}}$ is a local spin-dependent operator such as the spin density, $\hat{\rho}_m(\mathbf{x}) \equiv \sum_{\sigma=\pm1} \sigma \hat{\psi}^\dagger_\sigma(\mathbf{x})\hat{\psi}_\sigma(\mathbf{x}) \Big/ 2$.

We next assume that the matrix elements are antisymmetric with respect to the orbital index interchange, i.e. $O_{ab} = -O_{ba}$. Equation (5) then simplifies as

$$\begin{aligned}\langle\hat{\mathcal{O}}\rangle = &\frac{1}{\sqrt{2}}\left(f_1^* f_2 - f_2^* f_1\right)\left(O_{\overline{a}\overline{b}} + O_{ab}\right) \\ &+ \frac{1}{\sqrt{6}}\left(f_1^* g_1 - g_1^* f_1\right)\left(O_{\overline{a}\overline{b}} - O_{ab}\right),\end{aligned} \tag{6}$$

where we find that the first [second] term vanishes while the other one remains in general if $\hat{\mathcal{O}}$ is a spin antisymmetric [symmetric] operator and the coefficient $f_1^* g_1$ [$f_1^* f_2$] has nonvanishing imaginary part. Spin-antisymmetric [-symmetric] observables with respect to the MO index interchange include the spin [charge] flux, represented by $\mathbf{j}^m(\mathbf{x})$ [$\mathbf{j}^c(\mathbf{x})$], where the flux operators are defined as

$$\hat{\mathbf{j}}^m(\mathbf{x}) \equiv \frac{\hbar}{2im_e}\sum_\sigma \frac{\sigma}{2}\left(\hat{\psi}^\dagger_\sigma(\mathbf{x})\nabla\hat{\psi}_\sigma(\mathbf{x}) - \left(\nabla\hat{\psi}^\dagger_\sigma(\mathbf{x})\right)\hat{\psi}_\sigma(\mathbf{x})\right) \tag{7}$$

and

$$\hat{\mathbf{j}}^c(\mathbf{x}) \equiv \frac{\hbar}{2im_e}\sum_\sigma \left(\hat{\psi}^\dagger_\sigma(\mathbf{x})\nabla\hat{\psi}_\sigma(\mathbf{x}) - \left(\nabla\hat{\psi}^\dagger_\sigma(\mathbf{x})\right)\hat{\psi}_\sigma(\mathbf{x})\right), \tag{8}$$

respectively. We therefore find that, assuming the predominance of the SCF ground state configuration, *hybridization of local triplet excitations with nontrivial complex phase causes nonvanishing spin flux.*

In odd-electron systems, spin current also arises from single-electron excitations of the α or β spin electron. The most relevant α or the majority spin excitations are excitations of the SOMO, which we hereafter call as local doublet excitations. On the other hand, the β spin excitation to SOMO means, in the above example, a charge transfer (CT) from the A-B compound to the radical C. We next consider inclusion of a local doublet excitation term $h_1|\Phi^{(\mathrm{ldx})}\rangle$ and a charge transfer term $k_1|\Phi^{(\mathrm{CT})}\rangle$, defined as

$$|\Phi^{(\mathrm{ldx})}\rangle \equiv |a\overline{a}d\,\mathcal{C}\rangle \tag{9}$$

and

$$|\Phi^{(\mathrm{CT})}\rangle \equiv |a\overline{c}c\,\mathcal{C}\rangle, \tag{10}$$

respectively. Inclusion of these terms into the wavefunction Eq. (4), yields the following additional terms

$$\langle\hat{\mathcal{O}}\rangle|_{(\mathrm{ldx})} = f_1^* h_1 O_{cd} + f_1 h_1^* O_{dc}, \tag{11a}$$

and

$$\langle\hat{\mathcal{O}}\rangle|_{(\mathrm{CT})} = f_1^* k_1 O_{\overline{ac}} + f_1 k_1^* O_{\overline{ca}}, \tag{11b}$$

where the subscripts $|_{(\mathrm{ldx})}$ and $|_{(CT)}$ specify the origin of those contributions, local doublet excitation and the charge transfer, respectively. Notation $\langle\hat{\mathcal{O}}\rangle|_{(\mathrm{ldx})}$ [$\langle\hat{\mathcal{O}}\rangle|_{CT}$] represents contributions to the operator expectation value $\langle\hat{\mathcal{O}}\rangle$ arising from the ground state configuration $f_1\,|a\overline{a}c\,\mathcal{C}\rangle$ and the local doublet excitation $h_1|\Phi^{(\mathrm{ldx})}\rangle$ [charge-transfer term $k_1|\Phi^{(\mathrm{CT})}\rangle$]. For an operator $\mathcal{O}$ antisymmetric with respect to the orbital index exchange, they further simplify as

$$\langle\hat{\mathcal{O}}\rangle|_{(\mathrm{ldx})} = \left(f_1^* h_1 - f_1 h_1^*\right) O_{cd}, \tag{12}$$

and

$$\langle\hat{\mathcal{O}}\rangle|_{(\mathrm{CT})} = \left(f_1^* k_1 - f_1 k_1^*\right) O_{\overline{ac}}. \tag{13}$$

If the coefficient $(f_1^* h_1 - f_1 h_1^*)$ or $(f_1^* k_1 - f_1 k_1^*)$ has a finite imaginary part, Eq. (12) or Eq. (13) takes finite value for $\hat{\mathcal{O}} = \mathbf{j}^c$ and $\hat{\mathcal{O}} = \mathbf{j}^m$. For example, the local doublet excitation contributes the α spin current $\mathbf{j}^\alpha|_{(\mathrm{ldx})} = \hbar\,\mathrm{Im}\left(f_1^* h_1 - f_1 h_1^*\right)\left(\varphi_c\nabla\varphi_d - \varphi_d\nabla\varphi_c\right)/\,m_e$, which accompanies charge and spin flux as $\mathbf{j}^c|_{(\mathrm{ldx})} = \mathbf{j}^\alpha|_{(\mathrm{ldx})}$ and $\mathbf{j}^m|_{(\mathrm{ldx})} = \mathbf{j}^\alpha|_{(\mathrm{ldx})}\big/\,2$.

Thus it is concluded that, while *the local doublet excitations and the charge transfer, always accompany the charge flux in the same or opposite direction* with twice the amplitude, but those arising from *the local triplet excitations is not followed by the charge flux, i.e. these are pure spin fluxes.* The above analysis serves as a useful background to deconvolute the total flux from which states it results. We will show some of examples in Sec.3.2.4.

3. Flux analysis on the bond rearrangement in H· + H_2

3.1. Method of computation

3.1.1. Electron dynamics

We use the Semiclassical Ehrenfest Theory (SET) [31, 37, 38]. SET is based on the Ehrenfest dynamics, which combines the time-dependent Schrödinger equation for electronic degrees of freedom

$$i\hbar\dot{C}_I(t) = \sum_J \left(H^{\rm el}_{IJ}(\mathbf{R}_t) - i\hbar\dot{\mathbf{R}}\cdot\mathbf{X}_{IJ} \right) C_J(t) \tag{14a}$$

for the electron wavepacket Ψ_t expanded in CSFs as $\Psi_t = \sum_J C_J(t)\Phi_J$ and the mean-field forces working on nuclei given by

$$M^{(a)}\ddot{\mathbf{R}}^{(a)}_t = -\langle\Psi_t|\nabla^{(a)}_N H^{\rm el}(\mathbf{R})|\Psi_t\rangle, \tag{14b}$$

where $\mathbf{R}_t$ represents time-dependent nuclear coordinates in the supervector notation, $\nabla_N \equiv \partial/\,\partial\mathbf{R}$ represents the nuclear coordinate gradient, $\mathbf{X}_{IJ} \equiv \langle\Phi_I|\nabla_N|\Phi_J\rangle$ represents the derivative coupling of CSFs, $H^{\rm el}(\mathbf{R})$ represents the electronic Hamiltonian and the superscript (a) in Eq. (14b) specifies the nuclear index. Its advantage includes robustness, simplicity of implementation and smoothness of the nuclear dynamics, whereas it is known to breakdown in case where nuclear path–branching is essential [31, 32]. The reactions we work on this paper is essentially *adiabatic* and free from such branching. Nevertheless, even for such almost *adiabatic* reactions it is critically important to explicitly include nonadiabatic coupling operator in Eq. (14a) to attain the fluxes consistent with the time evolution of the related densities [12].

We have implemented SET into the GAMESS (US-GAMESS) package [39]. Static electronic states at each time step are calculated using the restricted open-shell Hartree Fock (ROHF) calculation followed by the graphical unitary group approach (GUGA) configuration interaction (CI) calculations. Our dynamical electronic wavefunctions are represented in a linear combination of the configuration state functions (CSFs) obtained in the CI calculation and evolves in time through operation of Hamiltonian and other matrices in CSF representation (see Eq. (14a)). MOs are expanded in a set of atomic orbitals (AOs) $\{\chi_\nu(\mathbf{r})\}$ as $\varphi_\ell(\mathbf{r}) = \sum_\mu \chi_\mu(\mathbf{r})\mathcal{C}^\mu_\ell$ with $\mathcal{C}^\mu_\ell$ representing the MO coefficients.

To evaluate the spin-dependent observables such as density matrices $\rho^\eta_{\mu\nu}$ with $\eta = \alpha, \beta, m$, we apply the method given in Ref. 40 to rewrite each CSF to a linear combination of Slater determinants.

At each time step, in addition to the CI calculation, we perform the coupled perturbed Hartree-Fock (CPHF) calculation to obtain MO coefficient derivative matrices $\mathbf{U}_{\ell m}$, defined as

$$\mathbf{U}_{\ell m} \equiv \sum_{\mu\nu} \mathcal{C}^\mu_\ell S_{\mu\nu} \nabla_N \mathcal{C}^\nu_m, \tag{15}$$

with $S_{\mu\nu}$ representing the AO overlap matrix, in order to calculate the MO derivative coupling $\mathbf{x}_{\ell m} \equiv \langle\varphi_\ell|\boldsymbol{\nabla}_N|\varphi_m\rangle$ through

$$\mathbf{x}_{\ell m} = \mathbf{G}_{\ell m} + \mathbf{U}_{\ell m}, \tag{16}$$

where $\mathbf{G}_{\ell m}$ is a transformation of the AO derivative coupling $\mathbf{x}_{\mu\nu} \equiv \langle\mu|\nabla_N|\nu\rangle$ in the sense $\mathbf{G}_{\ell m} \equiv \sum_{\mu\nu} \mathcal{C}^\mu_\ell \langle\mu|\nabla_N|\nu\rangle \mathcal{C}^\nu_m$. We also perform numerical differentiation of the CI Hamiltonian to obtain the gradient of Hamiltonian operator required for calculation of Eq. (14b) through the relation

$$\langle\Phi_I|\nabla_N H|\Phi_J\rangle = \nabla_N H_{IJ} - \sum_K \left(H_{IK}\mathbf{X}_{KJ} - \mathbf{X}_{IK}H_{KJ} \right). \tag{17}$$

The nuclear equation of motion shown in Eq. (14b) was integrated using the fourth order Gear integrator [41] with a fixed stepsize δt_N, whereas the electronic equation of motion, Eq. (14a) were

integrated with the 6th order Runge-Kutta integrator [42] with a stepsize $\delta t_{\rm el}$. Stepsizes δt_N and $\delta t_{\rm el}$ are specified later for each model.

We note the careful construction of the CI expansion in order to compromise flux conservation and the computational cost for the CI expansion, and practically we used full-CIS (fCIS) scheme proposed in Ref. [12].

3.2. H· + H_2 in collinear configuration

We below study radical reactions H· + H_2. The reaction has been regarded as one of the simplest prototypes of chemical reactions and has been extensively studied [43, 44] using advanced techniques including the quantum mechanical reactive scattering analysis. Here we do not work on reproducing accurate cross sections but concentrate on clarifying the flow of electrons upon bond rearrangement. In all these calculations, radical H· works as a projectile and is given a fixed initial velocity toward the molecular target. We define an initial reference geometry as the target molecule in the optimized geometry and the projectile located at a fixed spatial position with a predetermined initial velocity. The initial geometry of each trajectory is then constructed from the reference geometry by adding vibrational displacements and velocities on the target molecule setting randomly chosen initial phases on each vibration mode, thereby mimicking the zero-point vibrations. Yet, the resultant analyses presented below are to be made on the single trajectory basis but not in terms of a statistical average of multiple trajectories. Use of such distributed initial conditions is intended not for statistical sampling but for confirmation that the selected trajectory are not pathological. Each trajectory is therefore characterized by a set of initial nuclear coordinates and velocities.

3.2.1. Basis set

We suggested before that polarization functions should be included in the basis set used to minimize numerical flux nonconservation [12]. We here use the doubly polarized 3-21G basis [12], which is derived from the Pople's 3-21G basis set [45] by full uncontraction and augmentation by two sets of polarization functions with the same orbital exponents.

3.2.2. Dynamics

We first discuss the reaction of H· + H_2 in the collinear geometry, which is one of the simplest low-dimensional models of radical reactions. The projectile hydrogen radical is given the initial velocity along the collinear axis corresponding to the kinetic energy 1.0eV (see Fig. 1(a)). The integration stepsizes were $\delta t_N = 0.0375$ fs and $\delta t_e = \delta t_n/200$. Such excessively small stepsizes were chosen to take account of oscillatory nature of fluxes [12].

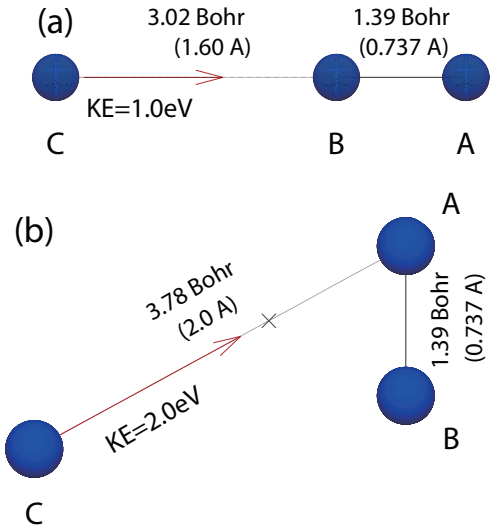

Figure 1: Initial geometry for the collision of (a) collinear and (b) triangular configurations.

Here we label MOs in the increasing order of orbital energy as $\varphi_1, \varphi_2, \cdots$, and define four types of CSF; the SCF ground state, $|\Phi_{I_0}\rangle = |\varphi_1\overline{\varphi_1}\varphi_2\rangle$, the charge-transferred (CT) state $|\Phi^{CT}\rangle = |\varphi_1\varphi_2\overline{\varphi_2}\rangle$, the local doublet excited states, $|\Phi^{ndx}\rangle = |\varphi_1\overline{\varphi_1}\varphi_{2+n}\rangle$ $(n = 1, 2, \cdots)$, the local singlet excited states, $|\Phi^{nsx}\rangle = |\sqrt{\frac{1}{2}}\left(\varphi_1\overline{\varphi_{2+n}} - \overline{\varphi}_1\varphi_{2+n}\right)\varphi_2\rangle$ $(n = 1, 2, \cdots)$, and the local triplet (in the sense we discussed in Sec. 2) excited state $|\Phi^{ntx}\rangle = |\sqrt{\frac{1}{6}}\left(\varphi_1\varphi_2\overline{\varphi_{2+n}} + \overline{\varphi_1}\varphi_2\varphi_{2+n}\right) - \sqrt{\frac{2}{3}}\varphi_1\overline{\varphi_2}\varphi_{2+n}\rangle$ $(n = 1, 2, \cdots)$. At $t = 0$, the lowest three MOs are characterized as the bonding MO of H_2, hydrogen $1s$-like orbital of the projectile and antibonding orbital of H_2, respectively. The above characterization of the state-components is valid only for the initial few femtoseconds though each MOs smoothly varies along the time evolution. However, the existence of the above extra electronic configurations such as $|\Phi^{CT}\rangle$, $|\Phi^{ndx}\rangle$, $|\Phi^{nsx}\rangle$, and so on with phase, is necessary for the non-vanishing spin fluxes to emerge.

3.2.3. Spin flux and the dynamics of spin density

Figure 2 shows the behaviors of the charge and spin fluxes along with the corresponding densities projected on the plane including the initial bond axis on it. As the spin density transfers from the projectile to the hydrogen atom in the other end, the current of spin is seen to flow from the projectile to the atom at the other end of molecule. It is also seen that the target hydrogen atom closer to the projectile attains negative spin density, which indicates cleavage of the original H_2 bond. The effect observed here is in harmony with the role of spin polarization discussed in much details in Ref. 46.

In the initial stage of dynamics, the electron flow tend to originate by $\alpha-$spin flux from a doublet excitation. Meanwhile, both the α and β spin flows in the opposite direction should have arisen from local triplet excitations. What we observe in this calculation is consistent with chemical intuition and with the basic scenario of the three-stage mechanism [34].

3.2.4. Spin flux assigned to electronic configurations

Before proceeding, we illustrate how the total spin flux can be deconvoluted to its components of the electronic configurations. According to the general method discussed in Sec. 2.2, the matrix elements for the spin flux arise between the SCF ground state configuration, $|\Phi_{I_0}\rangle$, and the higher configurations. Here we show the dominant four types of components given by the lowest energy, which are $|\Phi^{1dx}\rangle$ (the local doublet excitation), $|\Phi^{CT}\rangle$, $|\Phi^{1sx}\rangle$ (the local singlet excitation) and $|\Phi^{1tx}\rangle$ (the local triplet excitation). See Fig. 3, in which we find that each contributes flux proportional to $\varphi_j\nabla\varphi_\ell - \varphi_\ell\nabla\varphi_j$, with (j, ℓ) being $(2, 3)$, $(1, 2)$, $(1, 3)$ and $(1, 3)$ for $|\Phi^{1dx}\rangle$, $|\Phi^{CT}\rangle$, $|\Phi^{1sx}\rangle$ and $|\Phi^{1tx}\rangle$, respectively. In Fig. 3 are depicted the spatial distribution of $\mathbf{j}_{j,\ell}(\mathbf{r}) \equiv \varphi_j\nabla\varphi_\ell - \varphi_\ell\nabla\varphi_j$, with (j, ℓ) given above. Panel (b) in Fig. 3 particularly clarifies how the β spin flow is generated.

3.3. H· + H_2 in non-collinear configuration

We next study a non-collinear dynamics of the same system H· + H_2. As is shown in Fig. 1(b), the projectile is given an initial velocity corresponding to the kinetic energy 2.0 eV along a line that passes through the critical point, where the projectile makes an equilateral triangle with the target molecule at the reference geometry. The integration stepsizes were again set $\delta t_N = 0.0375$ fs and $\delta t_e = \delta t_n/200$.

We first exemplify one of the calculated trajectories, which is referred to as trajectory $\mathcal{A}$, along which bond-rearrangement undergoes. Figure 4 shows the snapshots of four types of fluxes and the corresponding densities calculated on the plane containing the triangle on it. We find that the spin current flows from the projectile C to the hydrogen atom A in the target molecule passing through the atom B (refer to Fig. 1(b).) It polarizes H_2 and there appears negative spin polarization around the atom B, which weakens the covalent bond between A and B. The behavior is therefore analogous to that found in the collinear dynamics. It is interesting to see that the intramolecular spin flow starts at earlier stage of the dynamics, $t \lesssim 6$ fs. In this time range, the atom C has not reached the equilateral point and is always closer to B. We can also confirm, in the second row of Fig. 4 corresponding to $t = 3.0$ fs, that all three types of spin flows suggested in Ref. 34 are taking place.

Since the quantum flux is a differential quantity, we often integrate it to attain information accumulated over wider areas and longer time, which is a standard practice in the study of electron current [47].

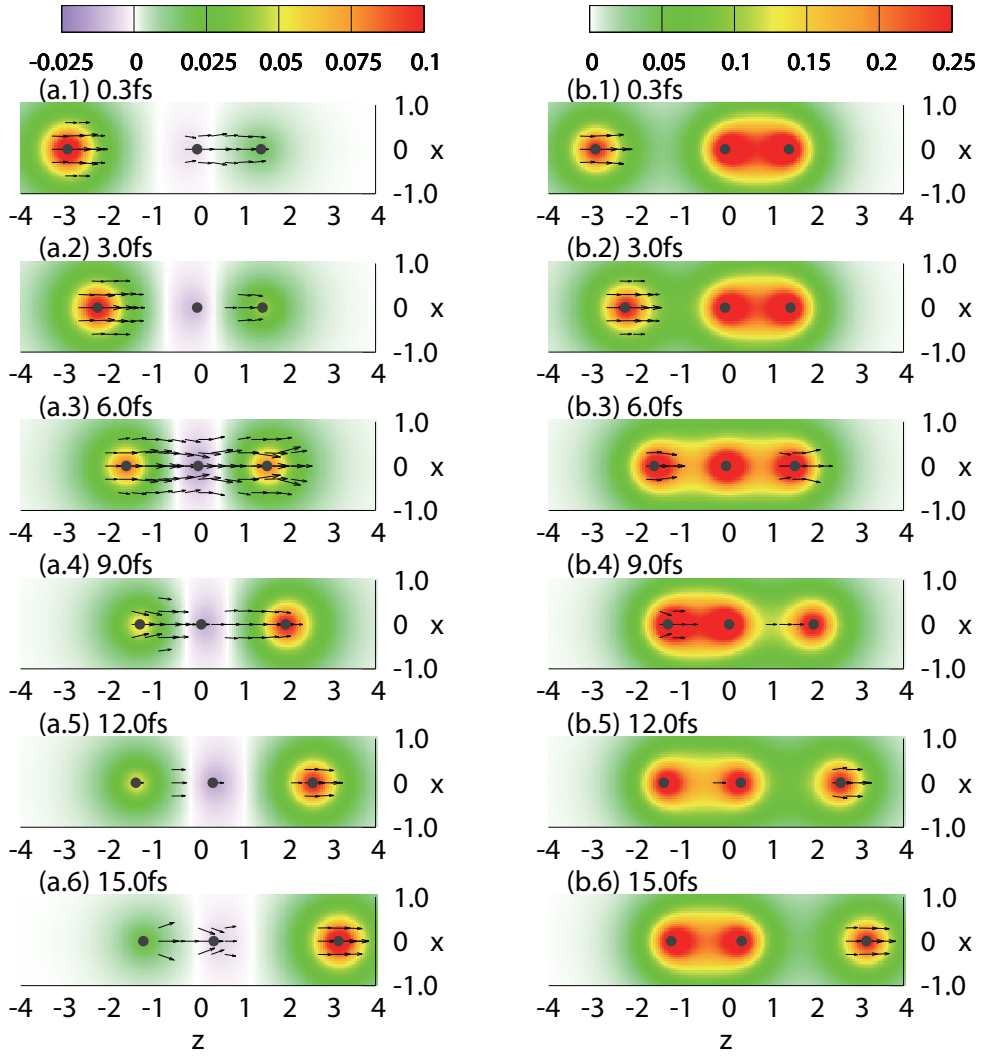

Figure 2: Snapshots of fluxes and densities in collinear bond rearrangement collision of H· + H_2.Panels to the left [right] show the snapshots of spin [charge] flux and density; black arrows show spin [charge] flux vectors which are overlaid on color plot of the spin [charge] density. Panels (a.1) to (a.6) [(b.1) to (b.6)] are the snapshots taken at time points $t = 0.15$, 3.0, 6.0, 9.0, 12.0 and 15.0 fs, respectively. The spin [charge] fluxes are evaluated on the spatial grid with spacing 0.3 Bohr and those with projected vector norm less than 2.5×10^{-4} a.u. [5.0×10^{-4} a.u.] are neglected. The remaining projected flux vectors, shown with black arrows, are scaled by a constant factor 1000 [500] to make them easier to see.

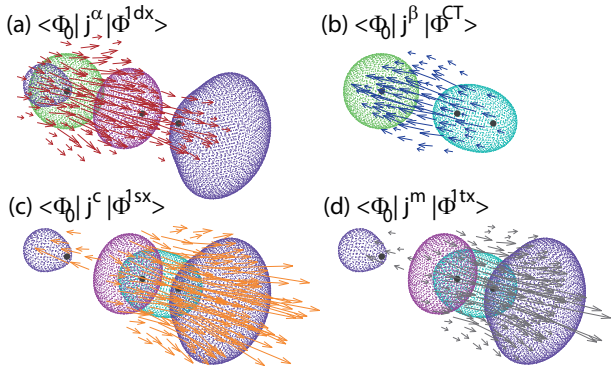

Figure 3: Schematic images of the fluxes arising from $|\Phi^{1dx}\rangle$ (a), $|\Phi^{CT}\rangle$ (b), $|\Phi^{1sx}\rangle$ (c) and $|\Phi^{1tx}\rangle$ (d). Arrows in each panel show the vector field $\mathbf{j}_{j,\ell}(\mathbf{r})$ defined in the main text. To make them easier to see, the vector fields in panels (a)-(d) are scaled by a constant factor, 100, −100, 200 and 100, respectively. Colors of the arrows, red, blue, orange and gray are representing α, β, charge and spin fluxes, respectively. The vector field $\mathbf{j}_{j,\ell}(\mathbf{r})$ is overlaid on the isocontour surfaces of the corresponding MOs, φ_j and φ_ℓ. Blue green and light green surfaces show the isocontour surfaces of φ_1 and φ_2, whereas blue-violet and red-violet surfaces show positive and negative isocontours of φ_3.

For instance, the following integrals

$$I_A^\eta \equiv -\int_0^t dt' \int_{\partial V_A} d\mathbf{S}\cdot\mathbf{j}^\eta(\mathbf{r},t') \tag{18}$$

are among them, where ∂V_A indicates a surface surrounding a space volume V_A. The flux conservation that $\Delta Q_A^\eta(t) \equiv Q_A^\eta(t) - Q_A^\eta(0)$ should equal to $I_A^\eta(t)$, where $Q_A^\eta(t) \equiv \int_{V_A} d^3\mathbf{r}\rho^\eta(\mathbf{r})$. We in fact have carried out those numerical integrations by setting three dividing surfaces as ∂V_A of three partitioned subspace surrounding the relevant atoms A, B, and C, individually. (Figures are not presented here due to space limitation.) The qualitative outcomes from these integrals are as follows. In the stage of the dynamics earlier that 9.0 fs, the α spin population increases in the region surrounding A atom, decreases in that surrounding C atom but stays almost constant in the region surrounding B atom. The relevant flux data shows that there is nonvanishing flux from the area of C atom to that of B atom, and that of B atom to that of A atom. We therefore see that the α spin flows from the area surrounding atom C to that of A through the B area. Secondly, the β spin, on the other hand, flows in the opposite direction. In the initial ~ 4.5 fs, cancellation between the α and β electron flows results in vanishing charge flux. The scenario is hence analogous to the collinear case. This behavior is expected, since the atom C is always closer to B than A . Weak coupling between A and C polarizes A and transfers β spin to region surrounding C atom.

We next pick another trajectory, referred to $\mathcal{B}$, which starts from the same reference geometry as $\mathcal{A}$ with a different set of vibrational displacement of H_2. A major qualitative difference is that $\mathcal{B}$ does not result in bond rearrangement after collision, in which the atom C comes closest to the target molecule at around 6 to 9 fs, but it gets scattered without bond rearrangement. We can then confirm, up to ~ 4 fs, the β spin flows from the region surrounding A atom to that surrounding C atom, either directly or via region surrounding B atom, whereas the α spin flows in approximately opposite direction, resulting in spin flow from the area of C to that of A (figure for it is not presented). In the later time, however, the β spin flux change the direction to reduce the spin polarization. The flow in the later stage becomes pure charge current without spin current arising from the nuclear motion. A clear difference between the trajectories $\mathcal{A}$ and $\mathcal{B}$ is found in that only a smaller spin polarization has appeared along the trajectory $\mathcal{B}$, which should have resulted in the failure of bond rearrangement.

4. Summary

We have shown the spin flux as a promising means to monitor dynamics of bond-rearrangement reactions. We showed, in Sec. 2, a microscopic mechanism of non-vanishing spin fluxes associated to bond rearrangement. Our formal theory was then demonstrated in illustrative sample radical reactions through

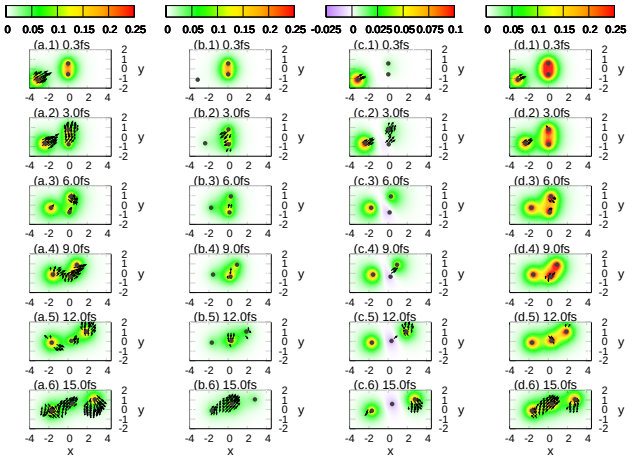

Figure 4: Snapshots of fluxes and densities in H· + H_2 along a trajectory $\mathcal{A}$ of non-collinear configuration, the quantities being projected on the triangular (molecular) plane. The alphabetical index on each panel distinguishes the type of flux/density; a to d corresponds to α, β, spin and charge, respectively, whereas the numerical index, specifies the time point of the snapshot; 1 to 6 correspond $t = 0.3$, 3.0, 6.0, 9.0, 12.0 and 15.0 fs, respectively. The color mapping of the density of each type is shown in the color bar on the top of each vertical row. Fluxes, evaluated on the spatial grid with spacing 0.3 Bohr and projected on the xy plane, are shown in arrows. The α β and spin fluxes [charge fluxes] with projected vector norm less than 2.5×10^{-4} a.u. [5.0×10^{-4} a.u.] are neglected. The remaining projected flux vectors, shown with black arrows, are scaled by factor 1000 [500] for easier visualization.

ab initio nonadiabatic dynamical calculations. Dynamical flow of spin in those reactions clarified roles of electron dynamics that modulate the local spin-state structures and bonding properties in molecules.

In this paper we treated the spin current as a theoretical issue, yet it is however worthwhile to briefly discuss possibility of experimental observation of the spin flux discussed in this paper. While there are a large number of reports [33] on observation of *macroscopic* spin currents in solids, observation techniques of *microscopic* fluxes in reacting molecules are not yet established. Observation of the latter should require, in addition to spin-resolved analysis, ultrashort time resolution of order femtoseconds or shorter and spatial resolution of atomic scale. We leave this problem to future studies. Yet, we are optimistic about future realization as there are pioneering studies of direct observation of *charge* currents using time-resolved X-ray scattering [48, 49] We believe the spin-flux analysis is also anticipated to shed light on the study of ultrafast spin dynamics.

Acknowledgments

One of the authors (K. T.) is deeply grateful to the late professor Kozo Kuchitsu for his long-standing dedication to the progress of physical chemistry and his interesting discussions. His own works on electron diffraction and low-energy electron scattering by molecules, what he called chemistry of electron beam, have been actually followed by the studies of electron dynamics in chemistry like ours. This work was supported mainly by JSPS KAKENHI (JP15H05752 and JP20H00373).

Data Availability Statement All data in this manuscript including computational settings are available upon reasonable request by contacting with the corresponding author. —

Conflicts of interest There are no conflicts of interest to declare.

Funding
JSPS KAKENHI (grant number JP15H05752 and JP20H00373).

References

[1] F. Pulizzi, Nature Materials 11 (2012) 367.

[2] N. Kumar, S. N. Guin, K. Manna, C. Shekhar, and C. Felser, Chem Rev. 121 (2021) 2780–2815.

[3] J. P. Lomont, S. C. Nguyen, and C. B. Harris, Acc. Chem. Res. 47 (2014) 1634–1642.

[4] Y. Jiang, L. C. Liu, A. Sarracini, K. M. Krawczyk, J. S. Wentzell, C. Lu, R. L. Field, S. F. Matar, W. Gawelda, H. M. Muller-Werkmeister and R. J. D. Miller, Nature Commun. 11 (2020) 1530.

[5] L. I. Schiff, Quantum Mechanics (McGraw-Hill, New York, 1955).

[6] L. D. Barron and A. D. Buckingham, Acc. Chem. Res. 34 (2001) 781–789.

[7] F. J. Adrian, Research on Chemical Intermediates, 3 (1979) 3.

[8] M. Okuyama and K. Takatsuka, Chem. Phys. Lett. 476 (2009) 109–115.

[9] K. Nagashima and K. Takatsuka, J. Phys. Chem. A 113 (2009) 15240–15249.

[10] T. Yonehara and K. Takatsuka, J. Chem. Phys. 144 (2016) 164304.

[11] R. Matuzaki and K. Takatsuka, J. Chem. Phys. 150 (2019) 014103.

[12] K. Hanasaki and K. Takatsuka, J. Chem. Phys. 154 (2021) 164112.

[13] I. Barth, H.-C. Hege, H. Ikeda. A. Kenfack, M. Koppitz, J. Manz, F. Marquardt, G. K.Paramonov, Chem. Phys. Lett. 481 (2009) 118–123.

[14] D. J. Diestler, A. Kenfack, J. Manz, B. Paulus, J. F. Pérez-Torres, and V. Pohl, J. Phys. Chem. A, 117 (2013) 8519-8527.

[15] T. Bredtmann, D. J. Diestler, Si-Dian Li, J. Manz, J. F. Pérez-Torrés, W.-J. Tian, Y.-B. Wu, Y. Yang, and H.-J. Zhai, Phys. Chem. Chem. Phys. 17 (2015) 29421.

[16] T. Schaupp, V. Engel, J. Chem. Phys. 151 (2019) 084309.

[17] A. Schild, Phys. Rev. A 98 (2018) 052113.

[18] G. Hermann, V. Pohl, J. C. Tremblay, B. Paulus, H. C. Hege, A. Schild, J. Comp. Chem. 38 (2017) 1515–1527.

[19] V. Pohl, L. E. M. Steinkasserer, J. C. Tremblay, J. Phys. Chem. Lett. 10 (2019) 5387–5394.

[20] J. Shao, V. Pohl, L. E. M. Steinkasserer, B. Paulus, J. C. Tremblay, J. Phys. Chem. C, 124 (2020) 23479–23489.

[21] S. Sobottka, M. Noesler, A. L. Ostericher, G. Hermann, N. Z. Subat, J. Beerhues, M. Behr-van der Meer, L. Suntrup, U. Albold, S. Hohloch, J. C. Tremblay, B. Sarkar, Chem. Eur. J. 26 (2020) 1314–1327.

[22] J. Shao, I. Alcon, B. Paulus, J. C. Tremblay, J. Phys. Chem. C 125 (2021) 25624–25633.

[23] F. Krausz and M. Ivanov, Rev. Mod. Phys. **81**, 163 (2009).

[24] P. M. Kraus, Y. Arasaki, J. B. Bertrand, S. Patchkovskii, P. B. Corkum, D. M. Villeneuve, K. Takatsuka, and H. J. Wörner, Phys. Rev. A **85**, 043409 (2012).

[25] I. Znakovskaya, P. von den Hoff, G. Marcus, S. Zherebtsov, B. Bergues, X. Gu, Y. Deng, M.J.J. Vrakking, R. Kienberger, F. Krausz, R. de Vivie-Riedle, and M.F. Kling, Phys. Rev. Lett. 108 (2012) 063002.

[26] K. Takatsuka, J. Chem. Phys. 146 (2017) 084312.

[27] K. Yamamoto and K. Takatsuka, Phys. Chem. Chem. Phys. 22 (2020) 7912-7934.

[28] Y. Arasaki and K. Takatsuka, J. Chem. Phys. 150 (2019) 114101.

[29] K. Hanasaki and K. Takatsuka, Phys. Rev. A 100 (2019) 052501.

[30] K. Hanasaki and K. Takatsuka, J. Chem. Phys. 151 (2019) 084102.

[31] T. Yonehara, K. Hanasaki, K. Takatsuka, Chem. Rev. 112 (2012) 499–542.

[32] K. Takatsuka, Bull. Chem. Soc. Jpn. 94 (2021) 1421–1477.

[33] Y. Kajiwara, K. Harii, S. Takahashi, J. Ohe, K. Uchida, M. Mizuguchi, H. Umezawa, H. Kawai, K. Ando, K. Takanashi, S. Maekawa and E. Saitoh, Nature 464 (2010) 262.

[34] S. Nagase, K. Takatsuka, and T. Fueno, J. Am. Chem. Soc. 98 (1976) 3838–3844.
(1952) 722–725.

[35] K. Fukui, Science 218 (1982) 747–754.

[36] V. Bonacic-Koutecky, J. Koutecky and L. Salem, J. Am. Chem. Soc. 99 (1977) 842.

[37] J. B. Delos and W. R. Thorson, Phys. Rev. A 6 (1972) 720–727.

[38] M. Amano and K. Takatsuka, J. Chem. Phys. 122 (2005) 084113.

[39] M.W. Schmidt, K.K. Baldridge, J.A. Boatz, S.T. Elbert, M.S. Gordon, J.H. Jensen, S. Koseki, N. Matsunaga, K.A. Nguyen, S. J. Su, T. L. Windus, M. Dupuis, J. A. Montgomery, J. Comput. Chem. 14 (1993) 1347–1363.

[40] G. Gidofalvi, R. Shepard, J. Comput. Chem. 30 (2009) 2414–2419.

[41] C. W. Gear, Commun. ACM 14 (1971) 176–179.

[42] W. H. Press, B. P. Flannery, S. Teukolsky and W. T. Vatterling, Numerical Recipes in C (Cambridge University Press, Cambridge, 1988)
.

[43] W. H. Miller, Annu. Rev. Phys. Chem. 41 (1990) 245–281

[44] D. Yuan, Y. Guan, W. Chen, H. Zhao, S. Yu, C. Luo, Y. Tan, T. Xie, X. Wang, Z. Sun, D. H. Zhang and X. Yang, Science 362 (2018) 1289–1293

[45] R. Ditchfield, W. J. Hehre, J. A. Pople, J. Chem. Phys. 54 (1971) 724–728.

[46] R. F. W. Bader, R. A. Gangi, J. Am. Chem. Soc. 93 (1971) 1831–1839.

[47] M. Okuyama, K. Takatsuka, Bull. Chem. Soc. Jpn. 85 (2012) 217–227.

[48] T. Bredtmann, M. Ivanov and G. Dixit, Nature Commun. 5 (2014) 5589.

[49] G. Hermann, V. Pohl, G. Dixit and J. C. Tremblay, Phys. Rev. Lett. 124 (2020) 013002